Effects of shock-induced cracks on the ultrasonic velocity and attenuation in granite

Huirong A. Ai[1] and Thomas J. Ahrens[1]

Received 16 February 2006; revised 30 July 2006; accepted 19 September 2006; published 9 January 2007.

[1] Measurements of the compressional wave velocity and the attenuation coefficients of 1-cm cubes were conducted. Samples were taken at various radii and depths beneath a 20 × 20 × 15 cm San Marcos granite block, impacted by a lead bullet at a velocity of 1200 m/s. The damage parameters of the cubes are calculated from the measured preimpact and postimpact P wave velocities, V_{p0} and V_p, and the crack density is inverted from the measured P wave velocities. The anisotropic orientation of cracks is more obvious from the attenuation than crack density and damage parameters calculated from the ultrasonic velocity. P wave velocity and the normalized distance from the impact point follow an exponential decay relation. Other properties, such as the damage parameter, crack density, and attenuation coefficient, are expressed by a power law decay with distance. The damage parameter and attenuation coefficients are approximately linearly related. The slope of the linear fitting results in directions normal to the crack orientation is about twice the value in direction along the crack orientation. The attenuation coefficient is found to be a more useful parameter than elastic velocity in describing the anisotropic orientation of cracks.

Citation: Ai, H. A., and T. J. Ahrens (2007), Effects of shock-induced cracks on the ultrasonic velocity and attenuation in granite, *J. Geophys. Res.*, *112*, B01201, doi:10.1029/2006JB004353.

1. Introduction

[2] Shock-induced damage and cracking beneath impact craters has become a focus of attention to those who use craters to study solar system history. Previous studies were conducted on small-scale craters in the laboratory [e.g., *Ahrens and Rubin*, 1993; *Polanskey and Ahrens*, 1990], as well as for large craters in the field, including both the Earth and the Moon [*Ackermann et al.*, 1975; *Dvorak and Phillips*, 1977; *Simmons et al.*, 1973]. The large-scale compressional wave velocity reduction in rocks beneath these impact craters has been attributed to the existence of cracks. Cracking in rocks can induce significant reduction of the effective elastic moduli of a fractured body, which, in turn, reduces the effective elastic wave velocities, as has been discussed for decades by many researchers both theoretically [*Eshelby*, 1957; *Nur*, 1971] and experimentally [e.g., *Ahrens and Rubin*, 1993; *Ai and Ahrens*, 2004].

[3] The damage parameter (D) and crack density (ε) are used to describe the intensity of fractures in the damaged body. Numerous theoretical models have been developed to relate the observed elastic velocity behavior to crack density of the cracked body. These models fall into two groups. One group of models assumes the volume concentration of inhomogeneities, such as cracks, cavities or inclusions with other properties in a homogeneous matrix, is small, such that the interaction between these inhomogeneities can be ignored [e.g., *Anderson et al.*, 1974; *Hudson*, 1990; *Kachanov*, 1993; *Nur*, 1971]. Another group of models takes into account the interaction between the inhomogeneities when the volume concentration of inhomogeneities is large [e.g., *Berge et al.*, 1993; *O'Connell and Budiansky*, 1974].

[4] The presence of cracks also affects the attenuation properties of the fractured body significantly. Attenuation mechanisms include friction, fluid flow and scattering, of which friction on thin cracks and grain boundaries is the dominant attenuation mechanism for consolidated rocks [*Johnston et al.*, 1979]. At ultrasonic frequencies, when the wavelength is at the same scale as heterogeneities in the rocks, scattering also plays an important role [*Tompkins and Christensen*, 2001].

[5] Attenuation phenomena have not yet received much attention by the planetary cratering community because of the difficulty of carrying out systematic attenuation measurements beneath impact craters in the field. *Liu and Ahrens* [1997] did preliminary work on attenuation beneath impact craters in the laboratory. They studied shock-induced damage in a San Marcos gabbro block and related the measured attenuation to the crack density and damage in the rocks. However, their work only measured the attenuation of the rocks in one direction, and did not take the orientation of the cracks and the propagation direction into account. In reality, the cracks produced by an expanding spherical shockwave within a target block include both concentric/spherical and tensile/radial cracks [*Polanskey and Ahrens*, 1990]. The combined effect of the heterogeneity of cracks on the attenuation is of interest in this study.

[1]Department of Geological and Planetary Science, California Institute of Technology, Pasadena, California, USA.

Copyright 2007 by the American Geophysical Union.
0148-0227/07/2006JB004353$09.00

Table 1. Mineralogical Composition of San Marcos Granite

Mineral	Area, %
Quartz	20.9
Plagioclase	51.0
Amphibole	25
Biotite	0.9
Opaque Fe_2O_3	0.9
Alkali feldspar	trace
Total	98.7

[6] In this work, the postimpact San Marcos granite target has been cut into 1-cm cubes. Compressional velocity as well as attenuation properties have been measured for these cubes using ultrasonic transmission and pulse-echo methods, respectively, in three directions. Section 2 discusses the experimental techniques, including the ultrasonic velocity and attenuation measurement methodology. Experimental results are presented in section 3, followed by the analysis and discussion of the experimental data. The measured stress wave velocities are used to calculate the damage parameter and crack density of the fractured rocks. The measured attenuation parameters are related to the crack information in the rocks.

2. Experimental Technique

[7] The San Marcos granite used in this study is from Escondido, California. Table 1 summarizes the mineralogical mode as obtained by analytical scanning electron microscopy (SEM) of a thin section. The grain size of quartz and plagioclase is 1 to 2 mm. These are intergrown with amphibole, biotite and opaque phases. On a microscopic scale, the rock is essentially crack-free except for microcracks along grain boundaries. The density of the San Marcos granite is 2.657 g/cm^3, the intrinsic compressional wave velocity is 6.31 ± 0.1 km/s, and the shear wave velocity is 3.65 ± 0.1 km/s, determined at 5 MHz.

[8] The initial 20 × 20 × 15 cm rock target was impacted by a lead bullet at a velocity of 1.2 km/s. The projectile has a radius of 0.3 cm and mass of 3.2 g. A 1-cm-thick center plane slice was cut from the recovered target, then 1-cm aliquots were cut from the plane. We assume that no additional cracks are produced by the cutting procedures. The cube surfaces were polished until the thickness variations of any two parallel surfaces reached ±0.005 mm. The residual water within the samples was largely removed by heating to 110°C for 24 hours within a vacuum furnace.

[9] The pulse transmission method [*Weidner*, 1987] was used for the ultrasonic velocity measurement. The PZT P wave transducers used were Model 1191, Panametrics, with a central frequency at 5 MHz. The signal was recorded with an oscilloscope (Gould 6500). Panametrics couplant D-12 is used for P wave measurements and alcohol as the couplant remover. The P wave velocity of the sample is given as

$$V_p = L/t_{\text{sample}} \tag{1a}$$

$$t_{\text{sample}} = t_m - t_{\text{ini}} \tag{1b}$$

where L is the length of the sample, t_m is the measured traveltime, and t_{ini} is the initial traveltime measured without the sample between the two transducers. Uncertainty of the traveltime measurement is ±0.02 μs. The calculated velocity has an error of 2% as estimated by the accuracy of the traveltime and length measurements.

[10] The pulse-echo technique described by *Winkler and Plona* [1982] was used to measure the attenuation coefficient. The transducer/sample assembly is shown schematically in Figure 1. The compressional wave transducer (Panametrics, Model V1191, central frequency 5 MHz) was placed inside a steel case so as to transmit the surrounding stress. A Panametrics 5052 UA pulser/receiver was used as the transducer's driver. Two Lucite buffers are used for coupling with the sample. The Lucite buffer plates were 1.3 cm in diameter, 0.6 cm in thickness for weak attenuation samples and 0.44 cm in thickness for stronger attenuation samples. The thickness of the buffer plates was chosen to avoid overlapping of the reflected waves from different surfaces. The Panametrics D-12 couplant was put between all the contact surfaces. A constant uniaxial stress load is applied through the position screw to the system to ensure good contact between the transducer/buffer and the buffer/sample surfaces. Stress waves reflected from surface A propagate in the first buffer plate only; waves reflected from surface B propagate through both the first buffer plate and the sample. The ultrasonic signals were recorded using a digital oscilloscope (Gould 6500). The signal was sampled at a period of 4 ns, and the amplitude resolution was 8 bits. Figures 2a and 2b are two typical signals showing the two reflected waves from surfaces A and B for the 0.6 cm and 0.44 cm thickness buffers, respectively. For the thin buffer, the first multiple from surface A is observed before the reflected wave from surface B (Figure 2b). Figures 2a and 2b also show the time windows for fast Fourier transform (FFT), ~1 μs, or 250 data points for surface A reflection, and ~0.7 μs, or 170 data points, for surface B reflection. Figure 3 shows the typical calculated relative spectral amplitudes.

[11] For a plane wave propagating in a solid medium, the amplitude of stress is given by

$$A(x,t) = A_0 e^{-\alpha x} e^{i(kx-\omega t)} \tag{2}$$

where x is propagation distance, ω is angular frequency, k is wave number, and t is time. The term of $A_0 e^{-\alpha x}$ represents

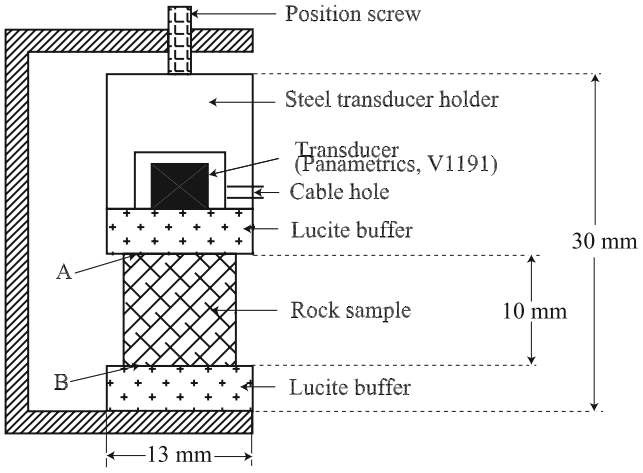

Figure 1. Sketch of attenuation measurement system (modified from *Winkler and Plona* [1982]).

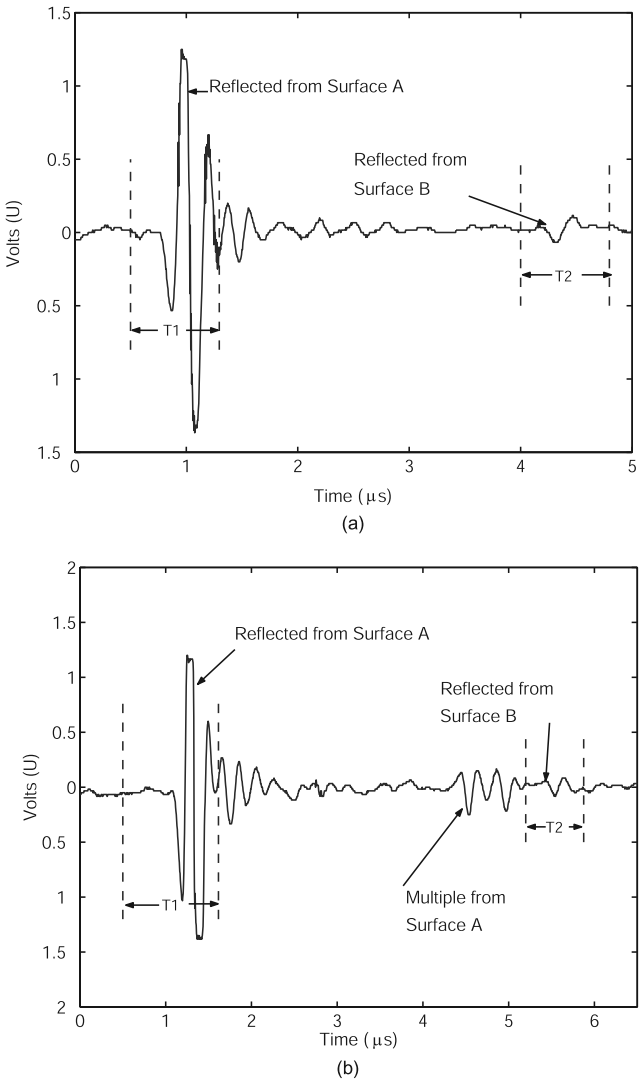

Figure 2. Typical ultrasonic record for attenuation measurements and spectral amplitude of signals. (a) For 0.6 cm thick buffer. Reflected wave from surfaces A and B are marked separately. T1 and T2 are time windows used for FFT analysis; and (b) for 0.44 cm thick buffer. Multiple reflection from surface A arrived before the first reflected wave from surface B.

the attenuation of the amplitude and α is the attenuation coefficient. A possible correction of attenuation due to wave spreading was not considered. According to *Winkler and Plona* [1982], α is calculated as follows:

$$\alpha(f) = \frac{8.686}{2L} \ln\left[\frac{A(f)}{B(f)}\left(1 - R^2\right)\right] \tag{3}$$

where L is the sample length and $A(f)$ and $B(f)$ are the frequency-dependent amplitudes of the pulse reflected from surfaces A and B of the sample, respectively. R is the reflection coefficient for the interface between the coupling buffer and sample, defined as

$$R = \frac{C_p\rho - C_{pc}\rho_c}{C_p\rho + C_{pc}\rho_c} \tag{4}$$

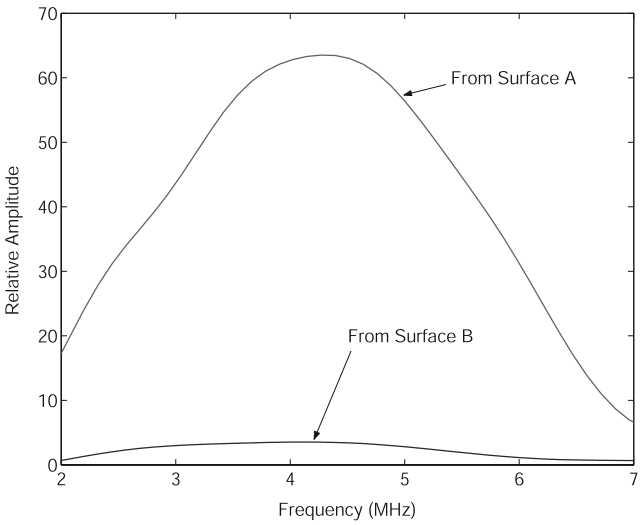

Figure 3. Calculated relative spectral amplitude of signals. Peak amplitude for surface A happens at frequency ~4.5 MHz.

where C_p and ρ are the P wave velocity and the density of the samples, respectively. Subscript c means the values for the Lucite buffers. In this study, C_{pc} is 2.68 ± 0.02 km/s and ρ_c is 1.19 g/cm^3.

3. Experimental Results

3.1. Compressional Wave Velocity Measurements

[12] The ultrasonic compressional velocity measurements for the granite cubes were measured in orthogonal directions (Table 2 and Figure 4). Unlike the results for the San Marcos gabbro from *Ahrens and Rubin* [1993], local seismic anisotropy associated to the major vertical fractures

Table 2. Compressional Wave Velocity Beneath Impact Crater in San Marcos Granite, Shot 117

	Radius From Crater Center Line x, cm								
Depth z, cm	0.5	1.5	2.5	3.5	4.5	5.5	6.5	7.5	8.5
				X Direction					
0.5	4.9	5.2	5.4	5.87	6.29	6.34	6.37	6.45	6.36
1.5	5.2	5.5	5.84	6.22	6.17	6.34	6.44	6.39	6.41
2.5	5.57	5.83	6.24	6.29	6.52	6.33	6.22	6.53	6.37
3.5	5.69	5.83	5.99	6.43	6.29	6.27	6.26	6.55	6.36
4.5	5.9	5.86	6.0	5.93	5.98	6.17	6.29	6.4	6.32
5.5	6.37	6.13	6.15	6.21	6.09	6.28	6.34	6.32	6.2
				Y Direction					
0.5	4.9	5.1	6.0	6.39	6.38	6.31	6.39	6.43	6.23
1.5	5.3	5.5	6.17	5.94	6.03	6.38	6.23	6.36	6.38
2.5	5.46	5.98	6.15	6.31	6.5	6.37	6.24	6.29	6.55
3.5	5.84	5.98	6.19	6.14	6.21	6.35	6.28	6.28	6.31
4.5	5.95	6.18	6.1	6.12	6.19	6.26	6.23	6.33	6.42
5.5	6.24	6.29	6.34	6.29	6.29	6.32	6.34	6.39	6.43
				Z Direction					
0.5	4.8	5.2	5.4	6.16	6.16	6.25	6.2	6.44	6.27
1.5	5.2	5.5	5.85	6.06	6.2	6.31	6.34	6.26	6.39
2.5	5.58	6.11	5.94	6.02	6.59	6.36	6.49	6.28	6.39
3.5	5.75	5.96	5.85	6.08	6.31	6.43	6.26	6.18	6.36
4.5	6.06	6.08	6.14	6.11	6.15	6.19	6.17	6.25	6.43
5.5	6.08	6.1	6.05	6.07	6.16	6.17	6.31	6.31	6.42

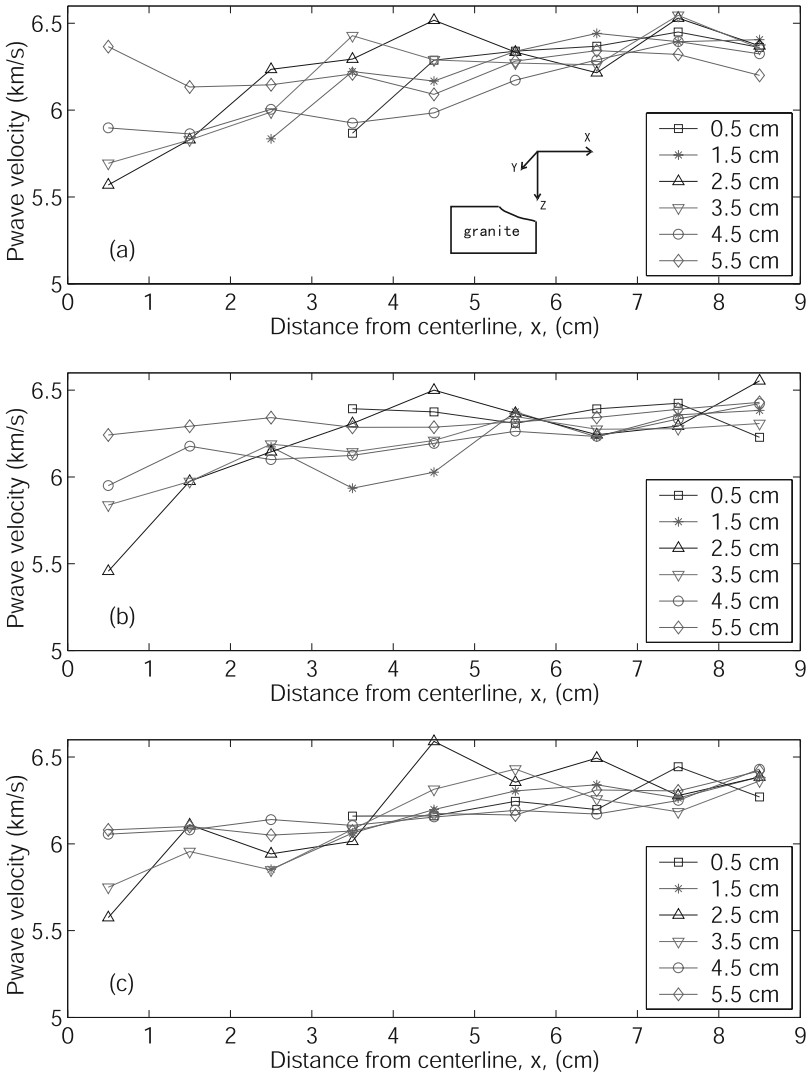

Figure 4. P wave velocities as a function of distance from z axis at indicated depths within sample in the (a) x direction, (b) y direction, and (c) z direction.

parallel with the specimen edge, or referred as ''side spallation fractures'' by *Fujiwara* [1980], is not observed. This is because the impact velocity, 1.2 km/s in our study, is much less than that used in *Ahrens and Rubin* [1993] for the gabbro shot. The unshocked intrinsic ultrasonic velocity value far from the crater center section is 6.4 ± 0.2 km/s for all the three directions (Figure 4). Beneath the center of the crater, the intrinsic velocity value is reached at a depth of 6 cm in the x direction; whereas for the z direction, which is the impact direction and contains the planar radial cracks beneath the crater, the intrinsic velocity is reached at ~4 cm. This phenomenon is more obvious in Figure 5. At a depth of 4.5 cm in the sample, the P wave velocity in the x direction is consistently lower than that in the z direction within the region near the crater center line. The P wave velocity approaches unshocked values at ~5.5 cm radial distance from the center line for all the three directions.

[13] Figure 6 shows the velocity measurements in all the three directions versus radial distance from the impact point, r ($r = \sqrt{x2 + z2}$). The relation between the P wave velocity and the radial distance, normalized by the radius of the projectile, 0.3 cm for this shot, is found to follow an exponential decay relation:

$$V_p = 6.24\left(1 - e^{(-0.26\pm0.01)r/r_0}\right) \quad (5)$$

[14] The ultrasonic P wave velocity increase to its unshocked value at r/r_0 equals 20, or, the radial distance ~6 cm. This is in good agreement with the observation of the limit of radial cracking that may be seen in the cross section after cutting the target open (Figure 7).

3.2. Attenuation Measurements

[15] Compressional wave attenuation coefficients are all calculated at a frequency of 4.5 MHz, the central peak of the reflected wave from surface A (Figure 3) using equations (3)–(4). The accuracy of calculating α_p using this pulse-echo method is estimated to be ±0.05 dB/cm [*Wepfer and Christensen*, 1990]. Figure 8 shows the relation between the attenuation coefficients versus the normalized radial dis-

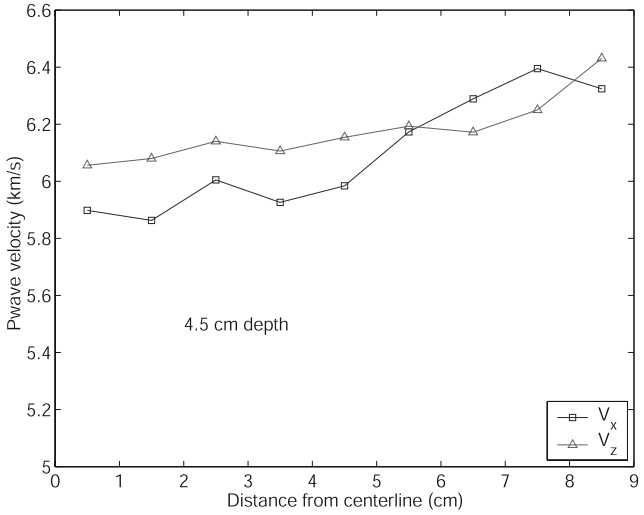

Figure 5. P wave velocities as a function of distance from z axis in x, y, and z directions at 4.5 cm depth below surface.

tance from the impact point. Nonlinear least squares fit of these data with the radial distance from the impact point follows a power decay law:

$$\alpha_x = (15.17 \pm 0.23)(r/r_0)^{-0.17\pm0.03} \tag{6a}$$

$$\alpha_y = (15.26 \pm 1.79)(r/r_0)^{-0.17\pm0.03} \tag{6b}$$

$$\alpha_z = (12.02 \pm 1.22)(r/r_0)^{-0.14\pm0.03} \tag{6c}$$

[16] The residuals (R^2) of the fittings are 0.56, 0.39, and 0.35, respectively. The scattering of the data is possibly caused by the coupling between the transducer and the sample surfaces, the heterogeneity of the rock samples, the limitation of the method itself, or a combination of all these reasons. Future steps should put emphasis on how to reduce the uncertainty of the measurement. However, although the data are scattered, the general trend indicates that the attenuation coefficients decrease with the increasing radial distance from the impact point. The attenuation coefficients in the x and y directions are similar to but different from those in the z direction. It is obvious from both the equations and Figure 8 that at the same distance from the impact point, attenuation parameters in the z direction are smaller than those in x and y directions. Therefore the amplitude of the compressional wave in the z direction attenuates less than those in the directions normal to the orientation of tensile cracks. This is because tensile cracks extend mostly in the z direction, and the effect of cracks on the amplitude of the ultrasonic wave is larger in directions normal to the orientation of the cracks, which are in the x and y directions, than that in the direction along crack orientation.

4. Analysis and Discussion

[17] For hypervelocity impact into brittle materials, both concentric/spherical and radial/tensile cracks are produced [*Polanskey and Ahrens*, 1990, Figure 5]. The radial cracks propagate further than the concentric cracks. This is because radial cracks are produced when the tensile stress in the elastic regime is greater than the tensile strength of the material, which is usually smaller, by a factor of ten, than the compressive strength. The compressional wave velocity is reduced substantially by cracks oriented with planes normal to the wave propagation direction [*Anderson et al.*, 1974; *O'Connell and Budiansky*, 1974]. In Figure 9, the plane of cracks extends in the z direction. The velocity of the compressional wave propagating in the x direction is reduced more than that propagating in the z direction. Therefore the reduction of the measured compressional wave velocity in the x direction by the tensile cracks is expected to be higher than that in the other two directions, which agrees with our results (Figures 4 and 5).

[18] The fracture of a cracked media can be described by two rather different but ultimately related parameters: (1) damage parameter, D, used by *Grady and Kipp* [1987] and *Ahrens and Rubin* [1993], defined as

$$D = 1 - \left(\frac{V}{V_0}\right)2 \tag{7}$$

where V and V_0 are the effective and intrinsic velocity of the fractured body, respectively; and (2) crack density, ε, expressed as

$$\varepsilon = N\langle a^3 \rangle \tag{8}$$

where N is the number of cracks per unit volume and $\langle a^3 \rangle$ is the average of the cube of the crack radii [e.g., *Kachanov*, 1993; *O'Connell and Budiansky*, 1974; *Wepfer and Christensen*, 1990].

[19] The two parameters are closely related. To relate fracture to material strength reduction, *Ashby and Sammis*

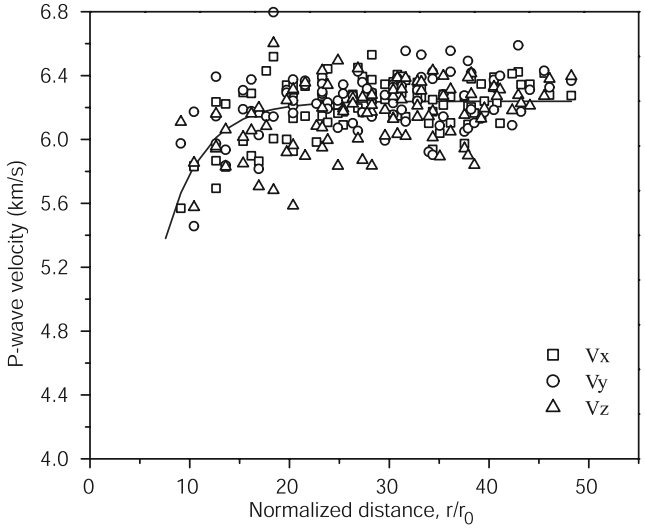

Figure 6. Plot of all velocity measurements in three directions as function of distance from crater center. Curve line is exponential decay fit of data. See equation (5).

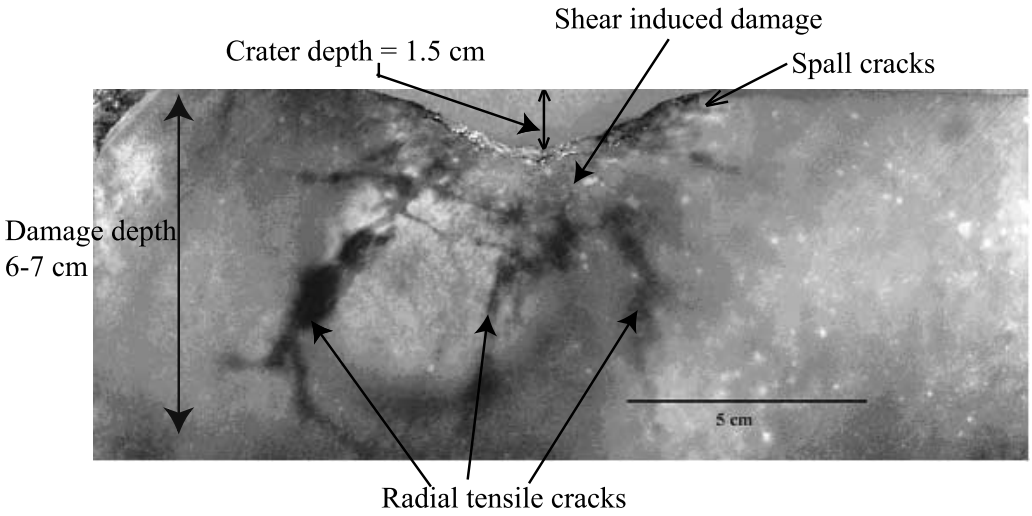

Figure 7. Cross section of shot 117, recovered granite impacted by 3.2 g lead bullet at 1200 m/s showing different types of cracks and damage depth. Cracks are highlighted by dye coolant.

[1990] give damage in a body with inclined cracks of length $2a$ by

$$D = \frac{4}{3}\pi(\alpha a)^3 N \tag{9}$$

where α is a geometric constant. It is obvious that this is the same concept as the crack density comparing equations (8) and (9). In this study, definition of damage parameter in equation (7) is used, since it is directly related to our velocity measurements.

[20] From the measured compressional wave velocity of the samples, D_p is calculated from equation (7). Figure 10 shows the damage parameter versus the normalized radial distance from the impact point for the three orthogonal directions. The data are fitted by a power decay law function:

$$D_x = (0.95 \pm 0.25)(r/r_0)^{-0.53\pm0.08} \tag{10a}$$

$$D_y = (0.99 \pm 0.22)(r/r_0)^{-0.54\pm0.06} \tag{10b}$$

$$D_z = (1.04 \pm 0.29)(r/r_0)^{-0.5\pm0.08} \tag{10c}$$

[21] The residuals (R^2) of the fittings are 0.58, 0.57 and 0.44 respectively. The damage parameters in all the three directions decay with distance from the impact point. Anisotropy is not very obvious from the damage parameter calculation.

[22] As mentioned before, the observed elastic velocity behavior of a rock is a function of the intrinsic elastic velocity, the matrix and fluid properties, the crack density (ε), the geometry of cracks and the interactions between them. In other words, crack density can be inferred from the observed elastic velocity provided the rest of parameters are known. Next we will use the theory of *O'Connell and Budiansky* [1974] to calculate the crack density using the measured compressional velocity. Usually the solution based on this type of model often does not correspond to experimental data for materials with a large contrast in component properties [*Levin and Markvo*, 2005]. Also, according to this model, the shear modulus becomes zero when the crack density is higher than a certain value. However, unlike another type of model [e.g., *Kachanov*, 1993], the model of *O'Connell and Budiansky* [1974] takes into account the interaction between cracks, which is important for rocks. Therefore the model of *O'Connell and Budiansky* [1974] is preferred for our study.

[23] Figure 11 shows the calculated crack density by using the model of *O'Connell and Budiansky* [1974] versus the normalized radial distance from the impact point for the three orthogonal directions. Similarly, the crack density decreases exponentially with the distance for all the three directions:

$$\varepsilon_x = 0.5(r/r_0)^{-0.58\pm0.09} \tag{11a}$$

$$\varepsilon_y = 0.5(r/r_0)^{-0.6\pm0.07} \tag{11b}$$

$$\varepsilon_z = 0.5(r/r_0)^{-0.54\pm0.08} \tag{11c}$$

[24] Again, the scattering of these data is caused by the same reason mentioned in section 3.2. Direct measurement of the crack damage using microscope will be carried out in the near future. The measurement can be compared with the calculated value here. This will be very useful to test the validity of the theocratical model of *O'Connell and Budiansky* [1974].

[25] Now we have both the damage parameter and the attenuation coefficient for the samples, it is interesting to explore the correlation between the two parameters. Figure 12 shows the dependence of attenuation coefficient on the damage parameter for the cubes measured in the three directions. The attenuation coefficients increase with

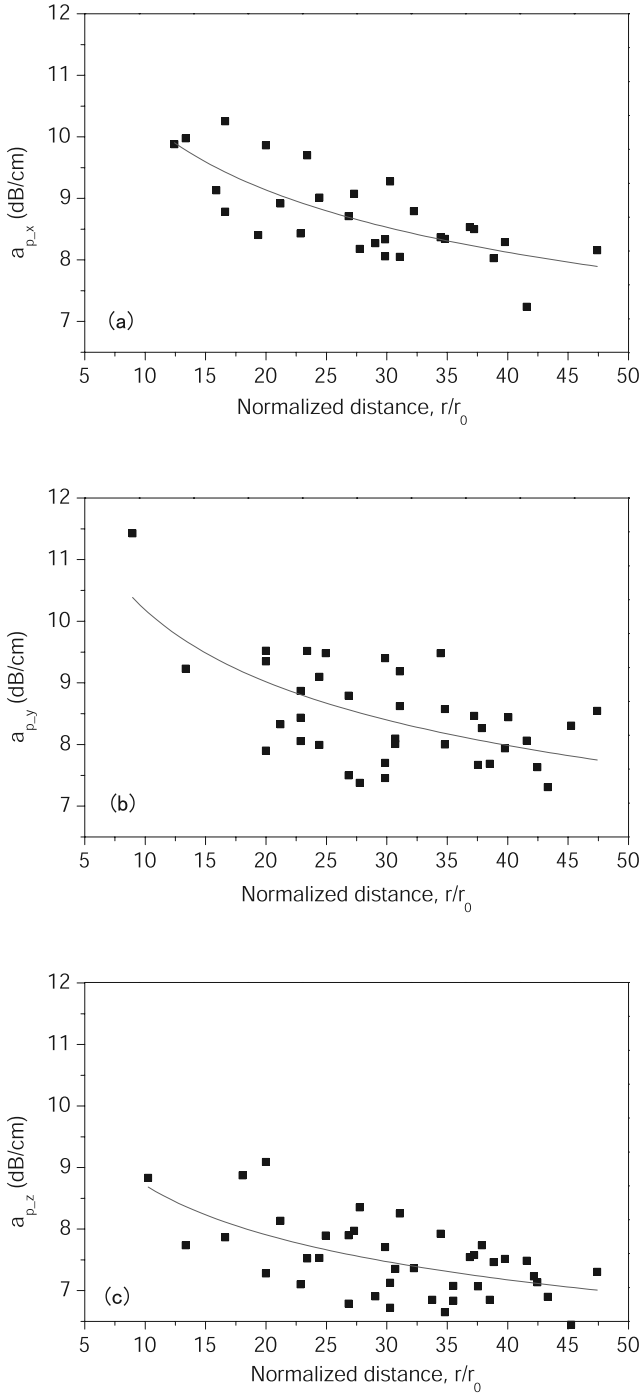

Figure 8. Attenuation coefficients as a function of normalized radial distance from impact point for three directions. Lines are power decay fit of data in the (a) x; (b) y; and (c) z directions.

the damage parameters consistently for the three situations. The data are fitted with

$$\alpha_x = 5.94 + (16.59 \pm 1.8)D_x \quad (12a)$$

$$\alpha_y = 5.66 + (17.09 \pm 1.6)D_y \quad (12b)$$

$$\alpha_z = 5.97 + (7.79 \pm 1.2)D_z \quad (12c)$$

[26] Unit of α is decibels per centimeter. The intercepts of these equations represent the intrinsic values of the attenuation coefficients of the samples when there is no shock-induced damage (D equals zero). The values for the three directions are very close (5.66 to 5.97). However, the slope of the equation for the z direction is only about half of the values of the x and y directions. This means that for the same damage parameter obtained from the measured P wave velocity, the attenuation coefficient in the z direction is smaller than the values in x and y directions. The tensile cracks propagating in the impact direction have a larger effect on the attenuation coefficients in directions perpendicular to it. Therefore the attenuation coefficient is a more useful parameter than the wave velocity in describing the anisotropic orientation of cracks.

5. Concluding Remarks

[27] The 1-cm cubes have been cut from a San Marcos granite target block recovered from an impact cratering experiment. Both compressional wave velocity and attenuation measurements were conducted on these cubes in three orthogonal directions. The damage parameter has been calculated from the measured P wave velocity. The theory of *O'Connell and Budiansky* [1974] was used to calculate the crack density of the cracked media from the measured velocity. The main conclusions obtained from this study are as follows:

[28] 1. Anisotropy is observed from the ultrasonic velocity and attenuation measurement, but it is not very obvious from the calculated damage parameter and crack density.

[29] 2. The measured P wave velocity and the normalized radial distance from the impact point follow an exponential decay relation, shown in equation (5).

[30] 3. The change of rock properties (D, ε, α) beyond the shock pressure regime 1 with the normalized radial distance from the impact point can be expressed by

$$(D, \varepsilon, \alpha) = \alpha(r/r_0)^b \quad (13)$$

where a and b are fitted constants.

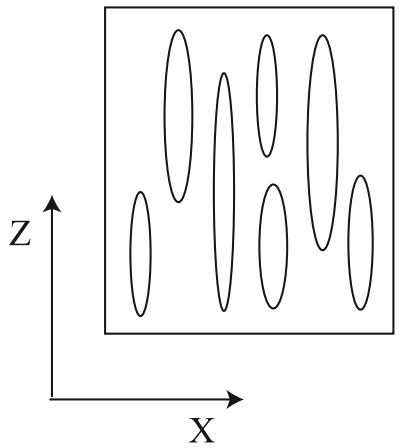

Figure 9. Schematic diagram showing effect of aligned cracks on elastic waves propagating at different directions. Compressional wave velocity in x direction is reduced more than that in z direction.

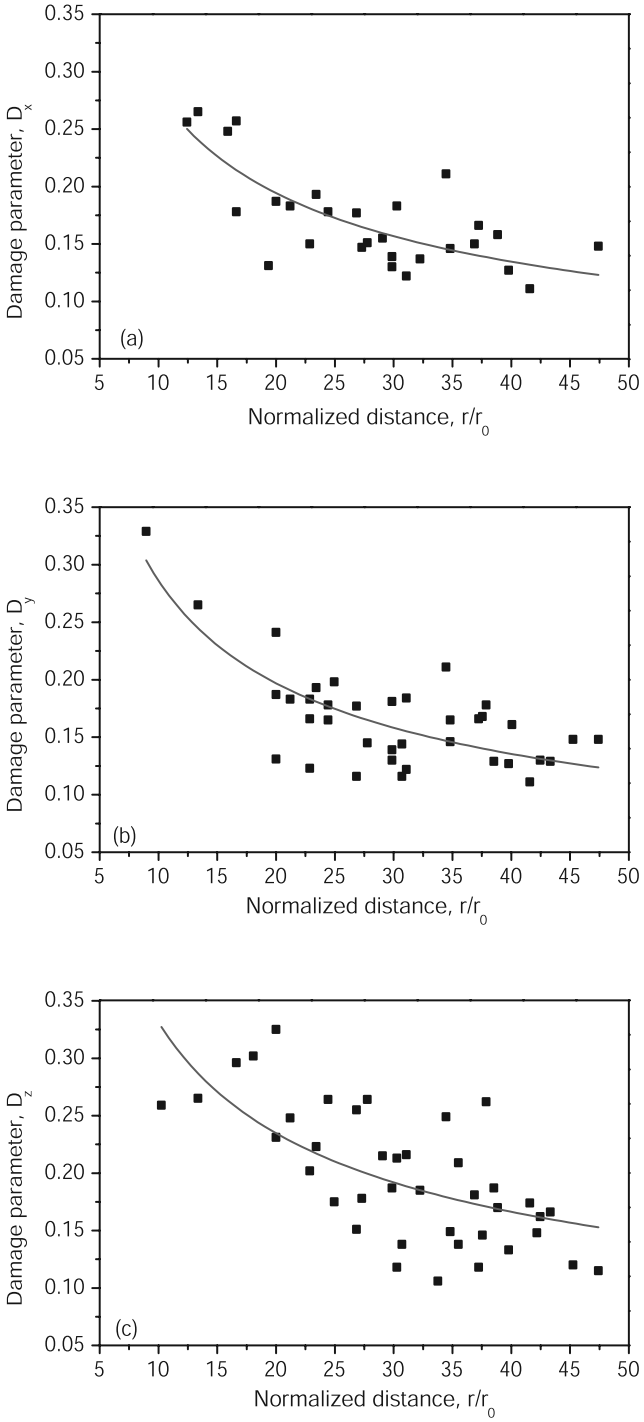

Figure 10. Damage parameters as a function of normalized radial distance from impact point for three directions. Lines are power decay fit of data.

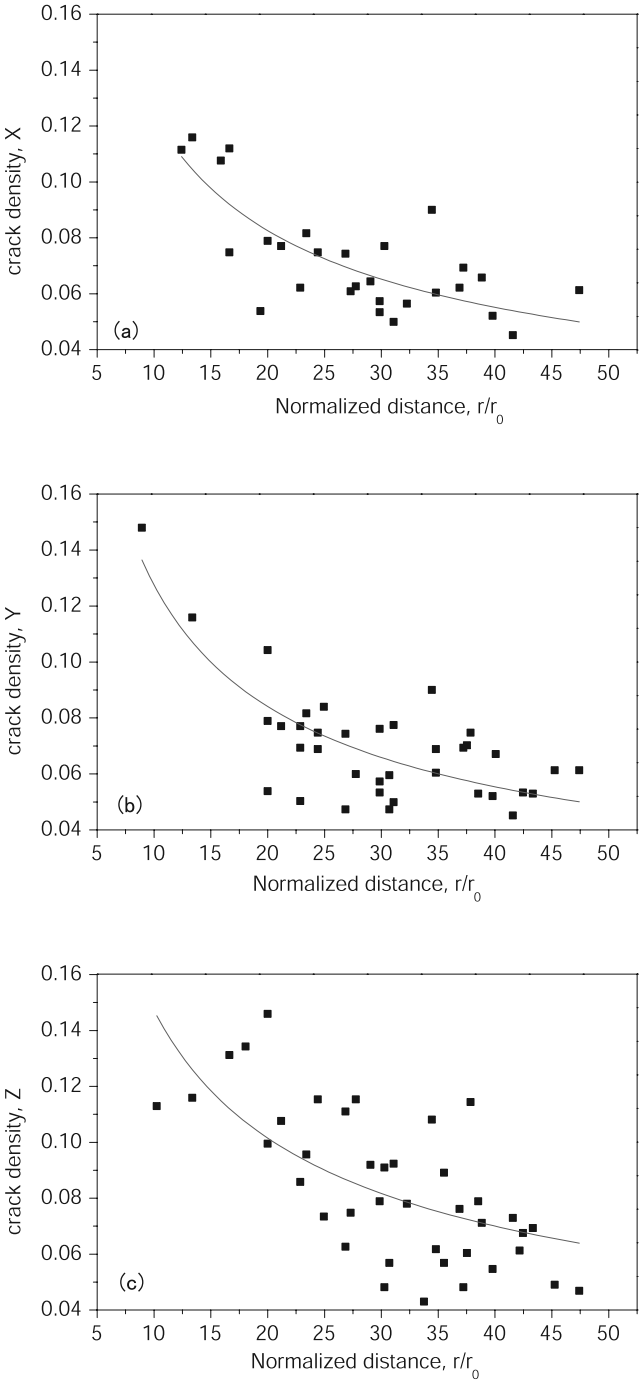

Figure 11. Crack densities inverted from measured P wave velocity by using model of *O'Connell and Budiansky* [1974] as function of normalized radial distance from impact point for three directions. Lines are power decay fit of data in the (a) *x*, (b) *y*, and (c) *z* directions.

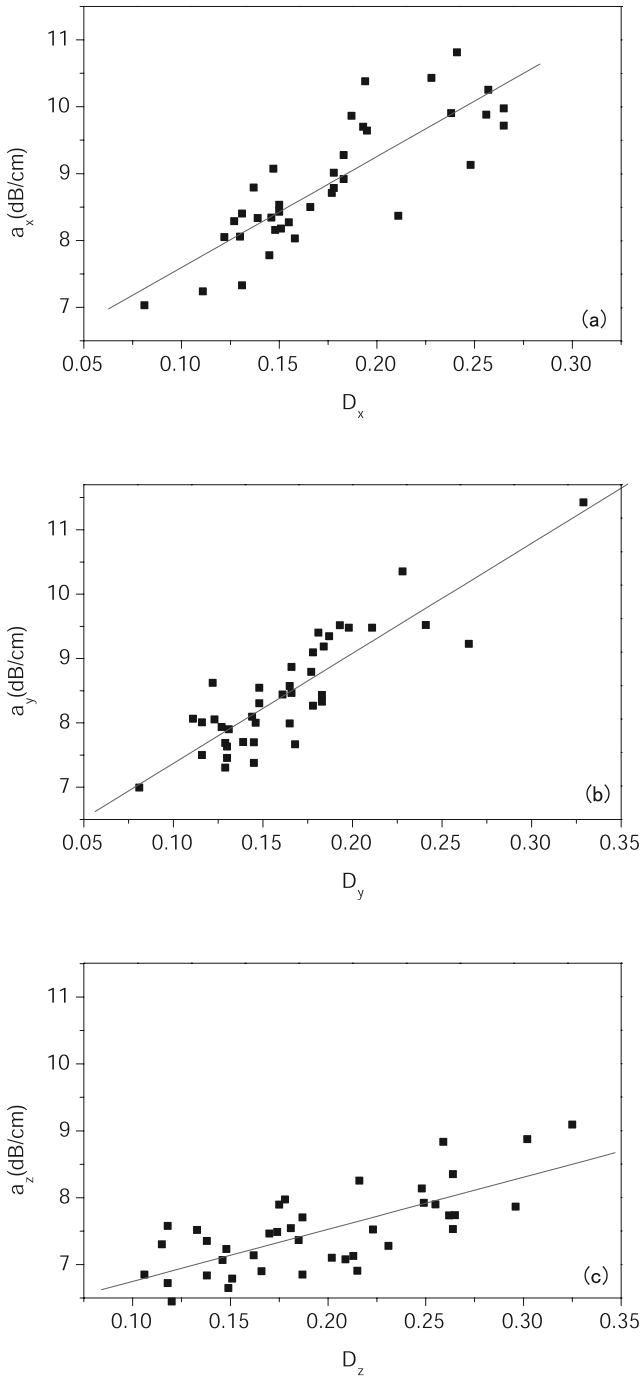

Figure 12. Attenuation coefficients versus damage parameter for the (a) x, (b) y, and (c) z directions. Lines are linear fit of data.

[31] 4. Attenuation coefficient is a more useful parameter than elastic velocity in studying the anisotropic orientation of cracks. From equation (12), the slope of the linear relation of attenuation coefficient versus damage parameter in the x and y directions is about twice that of the value in z direction.

[32] **Acknowledgments.** This research was supported by NASA Goddard grant under award NNG04GI07G. We appreciate the technical support of E. Gelle and M. Long. We thank G. Ravichandran for the use of the ultrasonic attenuation apparatus. We also thank Shiming Zhuang, Tracy Kidd, and Daoyuan Sun for their thoughtful suggestions and discussions. Division of Geological and Planetary Sciences, California Institute of Technology contribution 9128.

References

Ackermann, H. D., R. H. Godson, and J. S. Watkins (1975), A seismic refraction technique used for subsurface investigations at Meteor Crater, Arizona, *J. Geophys. Res.*, *80*, 765–775.

Ahrens, T. J., and A. M. Rubin (1993), Impact-induced tensional failure in rock, *J. Geophys. Res.*, *98*, 1185–1203.

Ai, H. A., and T. J. Ahrens (2004), Dynamic tensile strength of terrestrial rocks and application to impact cratering, *Meteorit. Planet. Sci.*, *39*(2), 233–246.

Anderson, D. L., B. Minster, and D. Cole (1974), The effect of oriented cracks on seismic velocities, *J. Geophys. Res.*, *79*, 4011–4015.

Ashby, M., and C. Sammis (1990), The damage mechanics of brittle solids in compression, *Pure Appl. Geophys.*, *133*, 489–521.

Berge, P. A., J. G. Berryman, and B. P. Bonner (1993), Influence of microstructure on rock elastic properties, *Geophys. Res. Lett.*, *20*, 2619–2622.

Dvorak, J., and R. Phillips (1977), The nature of the gravity anomalies associated with large young lunar craters, *Geophys. Res. Lett.*, *4*, 380–382.

Eshelby, J. (1957), The determination of the elastic field of an ellipsoidal inclusion and related problems, *Proc. R. Soc. London, Ser. A*, *241*, 376–396.

Fujiwara, A. (1980), On the mechanism of catastrophic destruction of minor planets by high-velocity impact, *Icarus*, *31*, 277–288.

Grady, D., and M. Kipp (1987), Dynamic rock fragmentation, in *Fracture Mechanics of Rocks*, edited by B. Atkinson, pp. 429–475, Elsevier, New York.

Hudson, J. A. (1990), Overall elastic properties of isotropic materials with arbitrary distribution of circular cracks, *Geophys. J. R. Astron. Soc.*, *102*, 465–469.

Johnston, D. H., M. N. Toksoz, and A. Timur (1979), Attenuation of seismic waves in dry and saturated rocks: I. Mechanisms, *Geophysics*, *44*, 691–711.

Kachanov, M. (1993), Elastic solids with many cracks and related problems, *Adv. Appl. Mech.*, *30*, 259–445.

Levin, V., and M. Markvo (2005), Elastic properties of inhomogeneous transversely isotropic rocks, *Int. J. Solids Struct.*, *42*, 393–408.

Liu, C., and T. J. Ahrens (1997), Stress wave attenuation in shock-damaged rock, *J. Geophys. Res.*, *102*, 5243–5250.

Nur, A. (1971), Effects of stress on velocity anisotropy in rocks with cracks, *J. Geophys. Res.*, *76*, 2022–2034.

O'Connell, R. J., and B. Budiansky (1974), Seismic velocities in dry and saturated cracked solids, *J. Geophys. Res.*, *79*, 5412–5426.

Polanskey, C. A., and T. J. Ahrens (1990), Impact spallation experiments: Fracture patterns and spall velocities, *Icarus*, *87*, 140–155.

Simmons, G., T. Todd, and H. Wang (1973), The 25-km discontinuity: Implications for lunar history, *Science*, *182*, 158–161.

Tompkins, M. J., and N. I. Christensen (2001), Ultrasonic p- and s-wave attenuation in oceanic basalt, *Geophys. Int.*, *145*, 172–186.

Weidner, D. J. (1987), Elastic properties of rocks and minerals, in *Methods of Experimental Physics*, edited by C. Sammis and T. Henyey, pp. 1–28, Elsevier, New York.

Wepfer, W., and N. Christensen (1990), Compressional wave attenuation in oceanic basalts, *J. Geophys. Res.*, *95*, 17,431–17,439.

Winkler, K., and T. Plona (1982), Technique for measuring ultrosonic velocity and attenuation spectra in rocks under pressure, *J. Geophys. Res.*, *87*, 10,776–10,780.

T. J. Ahrens and H. A. Ai, Department of Geological and Planetary Science, California Institute of Technology, MC 252-21, Pasadena, CA 91125, USA. (tja@gps.caltech.edu; huirong.ai@gmail.com)